A Temperature Instability in 4 K Cryocooler Regenerators Caused by Real Fluid Properties

R. Snodgrass[1], V. Kotsubo[2], J. Ullom[1,2], and S. Backhaus[1,2]

[1]National Institute of Standards and Technology, Boulder, CO 80305
[2]Department of Physics, University of Colorado Boulder, Boulder, CO 80309

ABSTRACT

We report temperature profile measurements from a densely instrumented, commercial pulse tube refrigerator. Azimuthal temperature differences of 15 K were measured across its 3 cm diameter regenerator which was operated at cold end temperatures below 10 K. These asymmetries may appear and disappear with just 0.1 K changes to the cold end temperature, suggesting a potential thermofluid instability. Experiments and analysis suggest that real fluid properties of helium at low temperatures may be the driving mechanism of the instability. We sketch the beginnings of a linear perturbation analysis and show that small changes to regenerator temperature profiles are reinforced by accompanying changes to the component of power flow due to real fluid properties, particularly at temperatures less than 9 K. Our measurements show that temperature asymmetries are specific to particular sections within the regenerator and negatively affect cooling power at the cold end.

INTRODUCTION

In low-temperature cryocoolers, real fluid properties[1,2] and finite solid heat capacity[3,4] can cause the temperature profile of regenerators to be far from linear.[5] For example, the temperature profile is usually flat at the cold end of the regenerator because near 4 K most power is carried by terms that are independent of temperature gradient. While the effect of real fluid properties on temperature profile has been considered previously in the literature, the possibility of instabilities arising from these properties has not yet, to the best of our knowledge, been observed or studied.

Instabilities exist in a variety of thermoacoustic machines. In refrigerators with large diameter regenerators, transverse, spatial variations in mass streaming and mean temperature couple[6] and reinforce each other, leading to an increased thermal load on the cold heat exchanger and reduced efficiency. Fluid diodes used in feedback pulse tube refrigerators[7] may be unable to suppress streaming in the direction of the acoustic axis if operated outside of a region of stability. Inverted pulse tubes have been compared to classical pendulums,[8,9] where gravity-driven convection may be suppressed if the acoustics are driven at high enough frequency. Each of these instabilities has been studied in the context of ideal gas working fluids. Below approximately 30 K, helium is strongly non-ideal, and its real fluid properties may also lead to instabilities.

An incomplete but intuitive understanding of an instability driven by real fluid properties is gained by considering the total power flow through the regenerator. One component of the total power is $\dot{H}_\beta=(1-T_m\beta)\,\dot{E}_2$. $\dot{E}_2$ is the acoustic power, which is always directed from the warm end of the regenerator towards the cold end; T_m is mean temperature; and β is the thermal expansion coefficient. In the ideal

Cryocoolers 21, edited by R.G. Ross, Jr., J.R. Raab and S.D. Miller

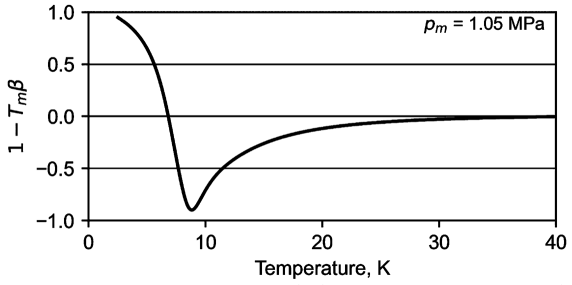

Figure 1. One minus mean temperature (T_m) multiplied by the thermal expansion coefficient (β) of helium-4 at a mean pressure of 1.05 MPa.

gas regime (roughly above 30 K) 1-$T_m\,\beta = 0$ and $\dot{H}_\beta$ does not carry significant power. In the real fluid regime 1-$T_m\,\beta$ is different from 0, and this term becomes important. Figure 1 displays a plot of 1-$T_m\,\beta$ versus T_m at 1.05 MPa. At this pressure, this mode of power flow is positive for $T_m < 6.8$ K and appears as a heat load on the cold heat exchanger, reducing the available cooling power. It is negative for $T_m > 6.8$ K and enhances the transport of heat away from the cold region toward the warm region. These strong shifts in the ability to move energy either toward or away from the cold end as temperature changes, from this and other related power flow terms, are a primary source of thermofluid instability.

As an example, consider an axial section of the regenerator at 15 K during cooldown to 4 K. If the temperature of one azimuthal half of the regenerator were increased in temperature to 16 K and the other azimuthal half were decreased to 14 K, the colder half will cooldown at a quickening pace because (1-$T_m\,\beta)\dot{E}_2$ is now more negative (increasing cooling power). In contrast, the half at 16 K cools at a relatively slower rate. These dynamic changes to the power flow will lead to diverging temperatures in the two halves of the regenerator that will continue until other power flow effects lead to saturation and a steady state.

In the remainder of this paper, we detail our experimental systems and procedures, describe our observations of a potential instability leading to azimuthal temperature asymmetries in the second-stage regenerator of a pulse tube refrigerator, and provide a preliminary perturbation analysis explaining how real fluid effects may be the mechanism driving the instability.

EXPERIMENTAL SYSTEM AND PROCEDURES

Figure 2 displays a schematic of our experimental system. Additional details of our experiment can be found in our group's second paper[10] for this conference. The system consists of a two-stage, commercial pulse tube refrigerator operating near 1.4 Hz. Our focus is on the second-stage regenerator that nominally spans temperatures from 40 to 60 K at its warm end to 2.5 to 10 K at the cold end. The diameter of the second-stage regenerator is close to 3 cm. We have densely instrumented the second-stage with 18 silicon diodes to measure the temperature at 9 axial locations along the regenerator using 2 diodes per axial location located on opposite sides of the regenerator. Each diode in a pair is mounted on one of two opposing copper clamps that mate around the regenerator shell. The two halves of each clamp are drawn together with two 4-40 stainless steel bolts but do not directly touch, so they are mostly thermally isolated from each other. The contact area between each clamp and the regenerator shell is an azimuthal band only 1.27 mm tall and slightly less than 180 degrees around the circumference. This small thermal contact patch minimally affects the temperature gradient along the regenerator. Two additional diodes are bolted directly to the copper of the warm and cold heat exchangers. All diode thermometers were calibrated to an accuracy of ± 25 mK at temperatures < 25 K and to ± 75 mK for higher temperatures. At the warm and cold heat exchangers we have placed heaters, which are integrated into a feedback system to control the warm (T_w) and cold end (T_c) temperatures to better than ± 20 mK. These control loops are utilized in all experiments reported here.

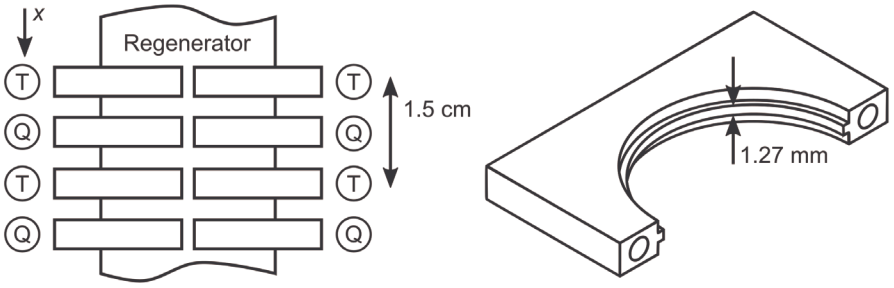

Figure 2. Schematic of the experimental test setup. Two opposing pieces of copper clamp around the second-stage regenerator tube (side view, left, and isometric view of one piece, right). A diode thermometer (T) is placed on each opposing clamp half so that the temperature of different regenerator halves can be compared. (Q) shows where we have the capability to apply intermediate heat, although we did not use this feature for the experiments presented in this paper.

In a typical experiment, the cryocooler is cooled down, the control loops for T_w and T_c are engaged, and the system is allowed to come into steady state. We then change T_c in 0.1 K increments in a step-like fashion, measuring temperature at all locations at a rate of roughly 0.5 Hz. We wait to proceed with the next temperature change until steady state is reached, this can take about 10 minutes if the temperature profile does not change drastically, or on the order of one hour if transitioning into or out of large temperature asymmetries. We scan T_c in 0.1 K steps near instability conditions in both directions, i.e. cooling down and warming up.

OBSERVATIONS

Figure 3a displays the maximum temperature asymmetry at any axial location along the regenerator when T_c is swept from 7.6 K to 6.2 K in increments of 0.1 K while holding T_w at 46 K. This maximum temperature difference is our measure of the asymmetry between the two halves of the regenerator. At higher values of T_c, the two halves of the regenerator display negligible asymmetry with small differences between the two halves of approximately 0.25 K. This asymmetry may be attributable to manufacturing variability. The dynamics of the cold end temperature following a 0.1 K step-like decrease in the control loop set point for T_c are shown in Figure 3b. Figure 3c shows the dynamic temperature evolution of the pair of thermometers on the clamps at $x/L = 0.8$, where x is

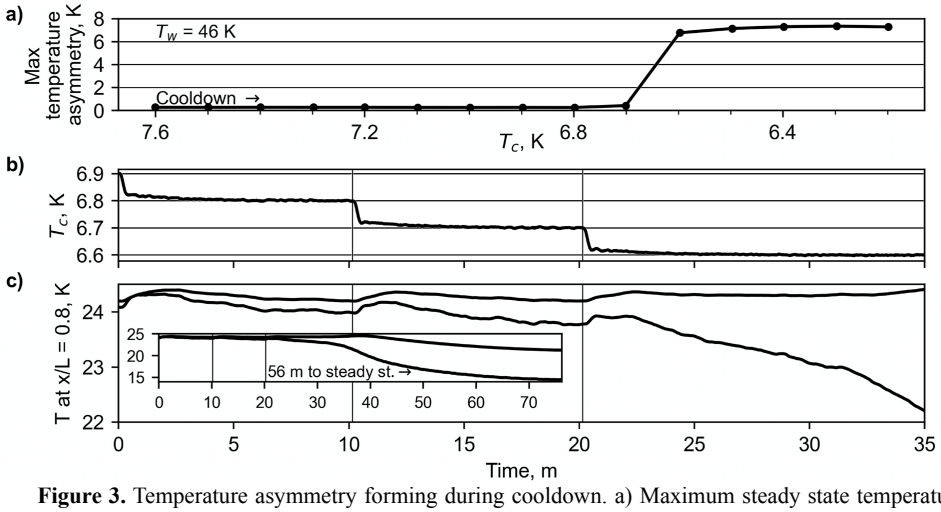

Figure 3. Temperature asymmetry forming during cooldown. a) Maximum steady state temperature difference between opposing thermometers at any axial location. Transient data for a subset of the data from a) are shown in b) and c). The cold end temperature is shown in b), and the temperature of opposing thermometers is shown for a particular regenerator location in c). Vertical lines show when T_c was changed.

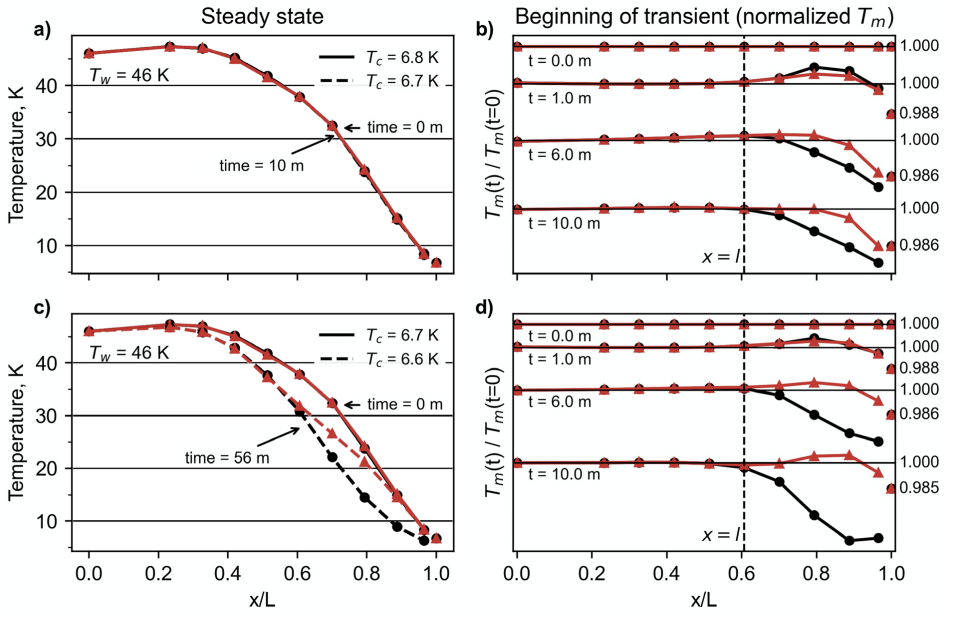

Figure 4. Cooling down the cold end in 0.1 K increments, demonstrating stability (top row) and instability (bottom row). Black lines with circular markers give the temperature of one azimuthal half of the regenerator; red lines with triangular markers give the opposite half. a) and c) give the steady state profiles, while b) and d) show the normalized temperature profile over time at four different timepoints. Straight horizontal lines on the right subplots give $T_m(t)/T_c(t=0) = 1$. The normalized distance along the regenerator is x/L, and $x = l$ is identified near Eq. 1. The profile shown in c) takes about 56 minutes to reach steady state after T_c change. The large temperature changes at 56 minutes are not shown in d) since they would obscure the important dynamics in the first 10 minutes after the change in T_c.

the distance along the regenerator axis starting at the warm heat exchanger and L is the total length of the regenerator. While in the stable regime with no large temperature asymmetry, the temperature profile in the middle of the regenerator reaches steady state within about 10 minutes after incrementing T_c (first two T_c steps in Figure 3b). When the cold end drops further to 6.6 K (third T_c step in Figure 3b), the temperature difference between the pair of thermometers at $x/L = 0.8$ grows from much less than 1 K to about 7 K over the course of about an hour. The sudden onset of this asymmetry is an indication of a thermofluid instability in the second-stage regenerator.

Figure 4 shows two T_c increments from Figure 3 but over the entire temperature profile, for $x/L = 0.0$ to $x/L = 1$. The steady state profiles for the last T_c step before instability are shown in Figure 4a (note: no noticeable change in temperature profile), and the dynamic transition between these profiles is shown in Figure 4b. Figure 4c and 4d show the same data for the first unstable step in T_c (note: a very large change in temperature profile). For the dynamic data in Figures 4b and 4d, the time-dependent temperatures are normalized by the steady-state temperature before the change in T_c to enhance the visibility of the dynamics. One minute after T_c is stepped down, the normalized profile looks similar for the stable step to 6.7 K (Figure 4b) as for the unstable step to 6.6 K (Figure 4d). In Figure 4d at six minutes after T_c is changed, the initial shape of the temperature profile that eventually leads to the larger asymmetry is clearly seen. In the next section, we will use an approximation to this observed shape as the start of a perturbation analysis.

Figure 5a shows maximum temperature asymmetry between the two regenerator halves over a wider range of T_c than presented in Figure 3. For the data in Fig. 5, the warm end is regulated to 54 K (somewhat warmer than in Figures 3 and 4) and the T_c increments are +0.1 K (instead of –0.1 K as in Figures 3 and 4). Over this wider range of T_c, there are multiple regions of large asymmetry with bordering regions of negligible asymmetry. Figure 5c shows the steady-state temperature profiles at values of T_c in each of these regions, which demonstrate that the temperature asymmetry can

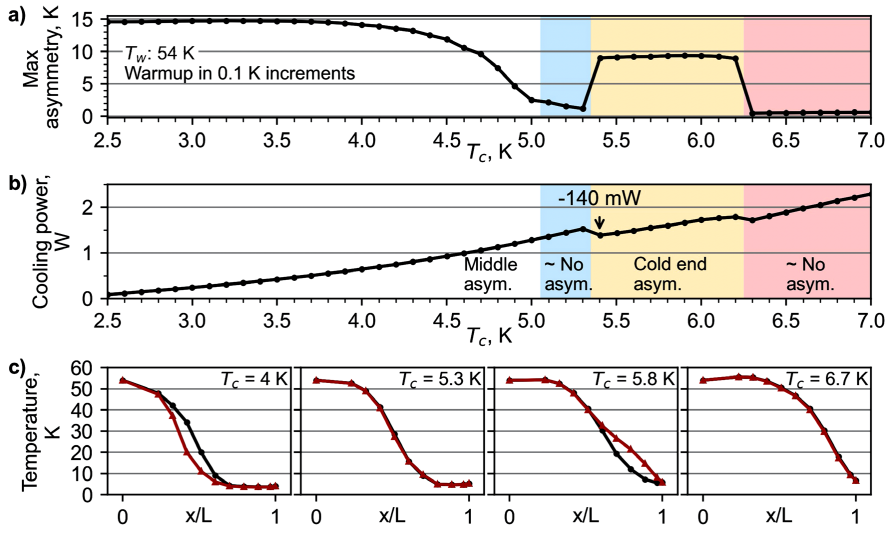

Figure 5. a) Maximum steady state temperature asymmetry as T_c is incremented up in 0.1 K steps while T_w is regulated to 54 K. b) Cooling power at the cold end for the same experiments in a). Colored shading shows the characteristic shape of the asymmetry for each T_c. c) Example temperature profiles for each shaded region in a) and b). Red and black lines represent the different halves of the regenerator.

exist within different parts of the regenerator. At the coldest temperatures, the asymmetry exists in the middle third of the regenerator. The asymmetry gradually fades as T_c approaches about 5 K. At T_c = 5.3 K, the asymmetry almost vanishes with the maximum temperature difference between halves at just 1.1 K (versus 14.7 K at T_c = 3.2 K). Raising T_c by just 0.1 K brings about a new asymmetry of about 9 K, but now the asymmetry resides in the coldest third of the regenerator. At T_c = 6.3 K and above the asymmetry at the cold end disappears just as abruptly as it appeared.

The cooling power $\dot{Q}_c$ at the cold heat exchanger for each T_c is shown in Figure 5b. There are discontinuities in $\dot{Q}_c$ when the asymmetry at the cold end appears and disappears. When raising T_c from 5.3 K to 5.4 K, we see a decrease in cooling power of 0.14 W, although we would normally expect cooling power to rise with increasing T_c. We do not observe any changes to cooling power at the cold end due to changes in the asymmetry in the middle of the regenerator, although it is possible that this asymmetry could affect intermediate cooling (cooling available along the regenerator itself is discussed more in our companion paper[10] for this conference).

The copper clamps we have mounted to the regenerator for temperature measurement likely cause the asymmetry to take a certain azimuthal orientation. Recall Figure 2, showing opposing copper clamps, each of which contact the regenerator around a circumferential band slightly less than 180 degrees. Since the copper clamps at different x locations are oriented identically (i.e. they are not randomly rotated), we expect that the clamps force the asymmetry to take the same orientation. We have made measurements where only two pairs of copper clamps were mated to the regenerator, and these pairs were modified so that each piece of copper contacted the regenerator over a small number of degrees. With the two pairs of small contact clamps, the asymmetry appeared at similar temperatures (differences in onset temperature between 0.1 K and 1 K versus experiments with many clamps) and produced temperature differences of similar magnitude to the measurements with many clamps. In the two pair configuration, we did observe signs that the asymmetry could rotate azimuthally (as was T_c incremented).

PRELIMINARY INSTABILITY ANALYSIS

The objective of our preliminary analysis is to reveal possible destabilizing influences that lead to temperature asymmetry. Our focus here will only be on the contribution from real fluid properties, we reserve a full analysis for future work. We start by considering a steady state symmetric temperature

profile, i.e., the same $T_m(x)$ in both regenerator halves. At time $t = 0$, we introduce a small temperature perturbation into the left half $\delta T_{m,left}(x, t = 0)$ and right half $\delta T_{m,rightt}(x, t = 0)$ of the regenerator (we are not concerned with the source of the perturbation). This perturbation causes changes to the power flows through the regenerator, which themselves cause changes to $\delta T_{m,left}(x, t = 0)$ and $\delta T_{m,rightt}(x, t = 0)$. The temperature and power flow perturbations become dynamic, and if the power flow perturbation reinforces the temperature perturbation, then the perturbation is unstable and grows into an asymmetry.

Analytical computation of the self-consistent shape of the temperature perturbation is beyond the scope of this work. Instead, we leverage the observed shape of the transient temperatures following a step change in T (see Figure 4d at $t = 6$ minutes). In this preliminary analysis, we estimate the shape as

$$\begin{aligned} \delta T_{m,left}(x,t) = -\delta T_{m,right}(x,t) = \delta T_0(t) \sin\left(\frac{\pi}{2}\frac{x-l}{L-l}\right) \quad & \text{for} \quad l < x < L \\ \delta T_m(x,t) = 0 \quad & \text{for} \quad 0 < x < l, \end{aligned} \tag{1}$$

where x is the distance along the regenerator axis, and $\delta T_0(t)$ is the amplitude of the perturbation, which may grow or decay with time depending on the relative balance of stabilizing and destabilizing effects. The perturbation begins at $x = l$ where the temperatures are the same, but where there is a difference in the temperature gradient between the left and right halves. For $x > l$ there is a temperature difference between the left and right halves that grows and takes on its largest value at the end of the regenerator at $x = L$, where the temperature gradients are the same.

The data in Figure 4d show similar behavior with the temperature deviation between left and right beginning near $x/L \sim 0.6$ (i.e., at $x = l$) and reaching a maximum at $x/L = 0.91$ or $x/L = 0.97$. The last data point in Figure 4d at x/$L = 1$ is recorded by a single diode that is bolted to the cold heat exchanger itself. Significant mixing of the helium as it flows through the cold heat exchanger likely homogenizes the temperature at that point, which is why in Figure 4 we have shown breaks in the temperature profiles at the cold end.

Our analysis of the power flows will use the thermoacoustic framework pioneered by Rott[11] and further developed by Swift[12]. Consider a simplified version of the total power equation:

$$\dot{H}_2(x) = \frac{1}{2}\mathrm{Re}\left[p_1 \widetilde{U_1}\left(1 - \frac{T_m\beta\left(f_\kappa - \widetilde{f_v}\right)}{(1+\epsilon_s)(1+\sigma)\left(1-\widetilde{f_v}\right)}\right)\right] + \dot{H}_T + \dot{H}_m + \dot{H}_\kappa, \tag{2}$$

where p_1 and U_1 are complex amplitudes of the oscillating pressure and volumetric flowrate, tilde represents the complex conjugate, σ is the Prandtl number, and $\epsilon_s = \phi\rho c_p/(1-\phi)\rho_s c_s$ is the ratio of the fluid to solid volumetric heat capacity in the regenerator (ϕ, ρ, c_p, ρ_s, c_s are the porosity, fluid density, fluid isobaric specific heat, solid density, and solid specific heat, respectively). The terms in H_2 with subscripts T, m, and κ are power flows carried by oscillating flow along a temperature gradient, steady flow (streaming), and thermal conduction, respectively. We do not write out those terms explicitly because here we will restrict our analysis to the first term in Eq. 2.

The thermoacoustic functions f_κ and f_v in Eq. 2 depend on the ratio of the hydraulic radius to the thermal penetration depth, i.e., r_h/δ_κ.[12] This ratio is expected to be of order 0.1 in highly effective low-temperature regenerators. Using expressions for f_κ and f_v in a parallel plate geometry as an approximation to porous media, we expand those expressions for small r_h/δ_κ and simplify the first power flow term in Eq. 2 to

$$\dot{H}_2(x) \approx (1 - T_m\beta)\dot{E}_2 + \left(\frac{\epsilon_s}{1+\epsilon_s}\right) T_m\beta\dot{E}_2 + \dot{H}_T + \dot{H}_m + \dot{H}_\kappa. \tag{3}$$

This form of the power flow equation splits the first term in Eq. 2 into components that do and do not depend on ϵ_s. In the temperature regime of interest ($T_m < 30$ K), 1-$T_m\beta$ is significantly different than 0. In practical cryocoolers, ϵ_s can be of order 1 across some or all of the second-stage regenerator. Therefore, we expect the two terms proportional to acoustic power $\dot{E}_2$ in Eq. 3 to carry a significant fraction of the total power flow in the region of the potential instability in Figure 4d. The effect of the temperature perturbation in Eq. 1 on these power flow terms plays a large role in determining if an instability arises.

Now we will continue our preliminary analysis by focusing our attention to the term that carries power when real fluid properties are most important, i.e. $\dot{H}_\beta = (1\text{-}T_m\beta)\dot{E}_2$. The response of this

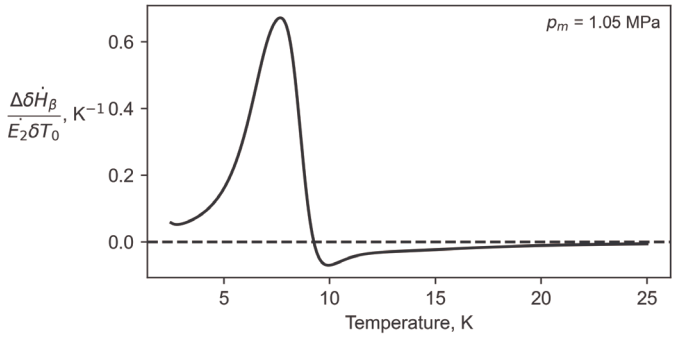

Figure 6. The power perturbation due to real fluid properties in the section of the regenerator between $x = l$ and $x = L$, normalized by acoustic power and the amplitude of the temperature perturbation.

power flow term to a temperature perturbation is

$$\delta\dot{H}_\beta = \delta T_m \, d\dot{H}_\beta / dT_m, \tag{4}$$

where the total derivative must be used because T_m, β and $\dot{E}_2$ are all dependent on T_m. The magnitude and time phasing of the oscillating (acoustic) pressure throughout the regenerator are typically constant, so that p_1 can be taken as real, and the acoustic power can be approximated as $\dot{E}_2 = p_1 \mathrm{Re}[U_1]/2$, so that the total derivative is

$$\frac{d\dot{H}_\beta}{dT_m} = \frac{\partial\dot{H}_\beta}{\partial T_m} + \frac{\partial\dot{H}_\beta}{\partial \mathrm{Re}[U_1]} \frac{\partial \mathrm{Re}[U_1]}{\partial T_m}. \tag{5}$$

Conservation of mass requires $\rho\mathrm{Re}[U_1]$ = constant. Differentiating this expression and using the definition $-\beta\rho = \partial\rho/\partial T_m l_p$, Eq. 5 is expressed

$$\frac{d\dot{H}_\beta}{dT_m} = \dot{E}_2 \left[\frac{-\partial(T_m\beta)}{\partial T_m} + (1 - T_m\beta)\beta \right]. \tag{6}$$

Combining this expression with Eq. 4, we can compute the power flow perturbation created by the temperature perturbation.

Next, we compute the joint time evolution of the temperature and power flow perturbations. Assuming that the fluid and solid are at the same temperature T_m, the perturbed energy equation requires

$$\left[\phi\rho c_p + (1-\phi)\rho_s c_s\right] A \frac{\partial \delta T_m}{\partial t} = -\frac{\partial \delta\dot{H}_\beta}{\partial x}, \tag{7}$$

where A is the cross-sectional area of the regenerator. Equation 7 reveals that these perturbations are not in steady state. Variations of the power flow perturbation along the regenerator axis will result in time varying accumulations of the energy in different regions of the regenerator, which drives time varying temperatures in those regions. A complete solution to Eq. 7 is beyond the scope of this preliminary analysis. Instead, we are guided by a simplified analysis used in other stability studies[7]. We begin by substituting $\delta T_m(x, t)$ from Eq. 1 into Eq. 7 and integrating from $x = l$ to $x = L$, which yields

$$C\frac{\partial \delta T_0(t)}{\partial t} = \delta\dot{H}_\beta(l) - \delta\dot{H}_\beta(L) \equiv \Delta\delta\dot{H}_\beta = \dot{E}_2 \left[\frac{\partial(T_m\beta)}{\partial T_m} - (1 - T_m\beta)\beta \right]_{x=L} \delta T_0(t). \tag{8}$$

The constant C in Eq. 8 is an average of the combined fluid and solid heat capacity weighted by the spatial dependence of the temperature perturbation. Equation 8 states the physically intuitive result that the amplitude of the temperature perturbation between $x = l$ and $x = L$ grows in time if the imbalance in the power flows at the two ends of the region create a net of power into the region, i.e., if $\delta\dot{H}_\beta(l) - \delta\dot{H}_\beta(L) > 0$. The difference $\delta\dot{H}_\beta(l) - \delta\dot{H}_\beta(L)$ in Eq. 8 is rewritten by setting $\delta\dot{H}_\beta(l) = 0$ (because $\delta T_m(x, t) = 0$ at $x = l$) and computing $\delta\dot{H}_\beta(L)$ by evaluating Eq. 6 at $x = L$, where $\delta T_m(x, t) = \delta T_0(t)$.

From Eq. 8, the amplitude of the perturbation $\delta T_0(t)$ grows exponentially in time when $\Delta\delta\dot{H}_\beta > 0$, where $\Delta\delta\dot{H}_\beta$ is given in the last term on the right-hand side of Eq. 8. Figure 6 displays $\Delta\delta\dot{H}_\beta$ as a function of the cold end temperature, i.e. $T_c = T_m$ $(x = L)$. For T_c less than about 9 K, $\Delta\delta\dot{H}_\beta > 0$. At these

temperatures, we predict that the original temperature perturbation grows due to perturbations to total power and is unstable. From this analysis, real fluid properties are a destabilizing mechanism at $T_m < 9$ K; however, analysis of the effect of $\delta T_m(x, t)$ on the other power flow terms is needed to make a more accurate prediction of the cold end temperature where perturbations become unstable.

DISCUSSION

Although we have shown how one term in the total power equation may promote temperature instability at low temperatures, each term in the power equation will have its own stabilizing or destabilizing contribution. For example, we have performed preliminary work that suggests the finite heat capacity term in the total power equation (i.e. the term containing ϵ_s in Eq. 3) largely promotes stability over the same temperatures that $\dot{H}_\beta$ promotes instability. A stabilizing influence from this term will push the threshold for transition to instability to a temperature colder than 9 K, which would be more in line with the transition temperature observed in our experiments. Because this ϵ_s term is highly dependent upon the regenerator material, it is likely that each cryocooler will exhibit this low-temperature instability differently.

Stabilizing effects from finite solid heat capacity may also be responsible for the compartmentalization of the asymmetry we see in Figure 5c. Since it is common for low-temperature regenerators to be constructed from multiple porous media, it's quite possible that we do not observe asymmetries between the middle third and coldest third of the regenerator because this location is a transition between materials. The lack of asymmetry might be explained by differences in the stabilizing effects from materials of dissimilar heat capacity, or by high-thermal-conductivity materials separating regenerator materials and promoting azimuthal temperature uniformity.

It is also important to note that the asymmetry onset is dependent upon more than just T_c. Consider the experiment in Figure 5, where the cold end asymmetry is not present at $T_c \geq 6.3$ K, while Figure 3 shows that the same asymmetry is not present at $T_c \geq 6.7$ K. The warm end temperatures for these experiments were 54 K and 46 K, respectively. This difference in onset temperature likely results from a difference in the stabilizing or destabilizing contributions from dT_m/dx terms in the total power equation ($\dot{H}_T$ and $\dot{H}_\kappa$ in Eq. 3). We have performed experiments with T_w up to 62 K. We generally observe stability at lower T_c with increasing T_w, suggesting that at least one of the dT_m/dx terms in Eq. 3 are stabilizing.

CONCLUSION

We have observed large temperature asymmetries (azimuthal temperature differences) in a low-frequency, low-temperature pulse tube refrigerator. The results presented here show that the asymmetry can be 15 K across a second-stage regenerator of just 3 cm diameter, which is a significant portion of the second-stage temperature span (~ 45 K). In other experiments not presented here, we have observed the asymmetry approach 19 K. The asymmetry appears to be restricted to certain regions of the regenerator – either the third of the regenerator closest to the cold end, or the middle third – which we believe to be a result of the transitions between different porous media. The onset of the asymmetry at the cold end depends sensitively on temperature (i.e. with changes to end conditions of just 0.1 K), while the asymmetry in the middle grows or disappears more gradually with changes to end conditions.

We also have presented the beginning of a linear perturbation analysis using transient measurements of the temperature profile to estimate the shape of the temperature perturbation that may lead to instability. We showed that the power flow term that depends strongly on the real fluid properties of helium ($\dot{H}_\beta$) promotes temperature instability at temperatures less than about 9 K. Some or all of the terms of the total power equation beside $\dot{H}_\beta$ likely promote stability; a complete perturbation analysis must consider all terms to fully explain stability criteria. Besides studying these other power terms and their influence on stability, we are currently in the process of performing a sweep of T_w and T_c to map out the stable/unstable state space.

Our work also demonstrates that accurately measuring the temperature profile of low-temperature cryocooler regenerators is not possible without considering azimuthal temperature variation.

ACKNOWLEDGMENTS

R. Snodgrass acknowledges support from a National Research Council Postdoctoral Fellowship. We would like to thank Greg Swift for stimulating discussion and leadership, and for assistance with the thermoacoustic software DeltaEC.

Figures were generated using Matplotlib and material properties were gathered using CoolProp[13], an open-source thermophysical library available as a Python wrapper.

Contribution of NIST, not subject to copyright.

REFERENCES

1. de Waele, A.T.A.M., Xu, M.Y., and Ju, Y.L., "Nonideal-gas effect in regenerators," *Cryogenics*, Vol. 39, no. 10 (1999), pp. 847–851.
2. Cao, Q., Qiu, L., and Gan, Z., "Real gas effects on the temperature profile of regenerators," *Cryogenics*, Vol. 61 (2014), pp. 31–37.
3. de Waele, A.T.A.M., "Finite heat-capacity effects in regenerators," *Cryogenics*, Vol. 52, no. 1 (2012), pp. 1–7.
4. Wang, C., "Numerical analysis of 4 K pulse tube coolers: Part I. Numerical simulation," *Cryogenics*, Vol. 37, no. 4 (1997), pp. 207–213.
5. Lang, A., Häfner, H.-U., and Heiden, C., "Systematic Investigations of Regenerators for 4.2K-Refrigerators" in *Advances in Cryogenic Engineering*, Springer US (1998), pp. 1573–1580.
6. So, J.H., Swift, G.W., and Backhaus, S., "An internal streaming instability in regenerators," *J. Acoust. Soc. Am.*, Vol. 120, no. 4 (2006), pp. 1898–1909.
7. Backhaus, S., and Swift, G.W., "An acoustic streaming instability in thermoacoustic devices utilizing jet pumps," *J. Acoust. Soc. Am.*, Vol. 113, no. 3 (2003), pp. 1317–1324.
8. Swift, G.W., and Backhaus, S., "The pulse tube and the pendulum," *J. Acoust. Soc. Am.*, Vol. 126, no. 5 (2009), pp. 2273–2284.
9. Carbo, R.M., Smith, R.W.M., and Poese, M.E., "A computational model for the dynamic stabilization of Rayleigh-Bénard convection in a cubic cavity," *J. Acoust. Soc. Am.*, Vol. 135, no. 2 (2014), pp. 654–668.
10. Snodgrass, R., Kotsubo, V., Ullom, J., and Backhaus, S., "Leveraging Real Fluid Effects as a Tool for Power Flow Measurements in 4 K Cryocooler Regenerators," *Cryocoolers 21,* ICC Press, Boulder, CO (2021), (this proceedings).
11. Rott, N., "Thermoacoustics," *Advances in Applied Mechanics,* Elsevier, Vol. 20 (1980) pp. 135–175.
12. Swift, G.W., *Thermoacoustics: A Unifying Perspective for Some Engines and Refrigerators*, 2nd ed. Springer International Publishing (2017).
13. Bell, I.H., Wronski, J., Quoilin, S., and Lemort, V., "Pure and Pseudo-pure Fluid Thermophysical Property Evaluation and the Open-Source Thermophysical Property Library CoolProp," *Ind. Eng. Chem. Res.*, Vol. 53, no. 6,(2014), pp. 2498–2508.